Characterisation and Modelling of the Reactions in a Three-Way PdRh Catalyst in the Exhaust Gas from an Ethanol-Fuelled Spark-Ignition Engine

C.McAtee[1], G. McCullough[1,*], D.Sellick[2], A.Goguet[3,*]

1. School of Mechanical and Aerospace Engineering, Queen's University Belfast, BT9 5AH, UK

2. Jaguar Land Rover Limited, Abbey Road, Whitley, Coventry CV3 4LF, UK

3. School of Chemistry and Chemical Engineering, Queen's University Belfast, BT9 5AG, UK

* Corresponding authors: g.mccullough@qub.ac.uk; a.goguet@qub.ac.uk

Abstract:

This work investigated and modelled the performance and characteristics of automotive catalytic converter formulations when subjected to a synthetic exhaust gas mixture representative of that emitted by an ethanol-fuelled spark-ignition engine. A synthetic gas reactor and exhaust gas emissions analysers were used to assess the catalytic activity, the products distribution and chemical mechanisms exhibited by a commercial catalytic converter formulation when exposed to ethanol containing gas mixtures. A commercially available after-treatment modelling platform named Axisuite was used to simulate the catalyst performance. This software was used to assign the pre-exponential frequency factor and activation energy variables within the rate equations. A set of global kinetic coefficients for the relevant reactions was established and is reported.

1. Introduction

Fossil fuel derived hydrocarbons (HCs) have been the primary source of energy for internal combustion engines for many years. Fluctuating crude oil prices, the desire for energy security and the increased desire for sustainable fuel sources, has driven the exploration for alternative fuel sources. Alcohols such as ethanol (C_2H_5OH) and methanol (CH_3OH) can be used in spark-ignition (SI) engines, and can be produced from various renewable sources.

Additionally, the presence of oxygen in alcohol fuels is advantageous as the emissions of carbon monoxide (CO) and unburned hydrocarbons are lower in comparison with traditional gasoline-fuelled engines (1, 2). Alcohol fuels have a higher octane rating than that of gasoline, which facilitates an increase in compression ratio in an engine optimised for alcohol fuel usage. The increased compression ratio improves thermal efficiency and provides a further reduction of pollutant emissions (3, 4). C_2H_5OH can either be used as an oxygenate source in gasoline (up to 10 vol%), without modification to engine components or operating parameters, or as the main fuel component in blends such as E85. The use of alternative fuels alters the engine out gas composition compared to that seen for gasoline fuelled vehicles. However, vehicles that use alternative liquid fuels still need to comply with the same emissions legislation as those vehicles fuelled by gasoline only.

Investigations into the effect of fuel C_2H_5OH content on exhaust composition reveal an increase in oxygenated species emissions, particularly C_2H_5OH and acetaldehyde (CH_3CHO) (5, 6, 7, 8**,** 9**)**. However, there is wide variation in reported results, which may be due to various reasons such as engine set-up, test conditions and whether the engine has been optimised for operation using E85 fuel. While numerous researchers have studied the kinetics of the combustion of ethanol within the cylinder, and therefore predicted the emissions resulting from this combustion (10), investigation of the reaction pathways within catalytic converters is limited.

The after-treatment system applied to a SI engine is in the form of a three-way catalytic converter (TWC) which contains platinum (Pt), palladium (Pd) and rhodium (Rh). Whilst E85 combustion can result in lower emissions of regulated pollutants such as CO, the generation and catalytic conversion of pollutants such as CH_3CHO requires increased understanding.

The activity of noble metal catalysts for C_2H_5OH and CH_3CHO control has been reported by several researchers. Maunula et. al (11) reported that PtRh and PdRh TWC formulations

displayed similar overall conversion efficiencies. However, PtRh showed a higher total hydrocarbon (THC) conversion efficiency and greater durability.

Lupescu et al. (7) studied the mechanism of C_2H_5OH conversion and subsequent CH_3CHO formation over zeolite catalysts/traps. The authors attribute CH_3CHO formation to partial oxidation of C_2H_5OH as shown in Equation 1, followed by methane (CH_4) formation which was attributed to the breakdown of CH_3CHO as shown in Equation 2.

$$C_2H_5OH + \frac{1}{2}O_2 \rightarrow CH_3CHO + H_2O \quad \text{Eq. 1}$$

$$CH_3CHO \rightarrow CH_4 + CO \quad \text{Eq. 2}$$

There is some discussion in the literature on the mechanisms by which CH_3CHO and CH_4 are generated from C_2H_5OH. Some assign CH_3CHO formation to CH_4 partial oxidation (7),(11),(12). An alternative mechanism is the dehydrogenation of C_2H_5OH to form CH_3CHO and H_2 as shown in Equation 3.

$$C_2H_5OH \rightarrow CH_3\mathrm{CHO} + H_2 \quad \text{Eq. 3}$$

The dehydrogenation and decomposition reactions have been observed at temperatures as low as 80°C (13, 14).

Physical testing of catalyst performance can be cost and time intensive which makes the use of modelling tools to predict catalyst behaviour very attractive. The requirement of a catalytic converter model is to accurately simulate the performance of the catalytic converter through mathematical representation of the physical and chemical processes that occur within it. These processes include mass transfer, heat transfer, and the surface reactions associated with the chemical reactions of interest. While numerous catalyst models have been reported in the literature, such as those by Kuo *et al.* (15), Voltz *et al.* (16) and Montreuil *et al.* (17),

limited information is available regarding the reactions that occur on a catalyst exposed to the exhaust gas of an ethanol-fuelled SI engine.

Stepanek et. al. (12) reported a global kinetic model which incorporated rate equations as derived from experimental synthetic bench testing. The authors described reaction pathways in oxygen rich exhaust gases which included partial oxidation of C_2H_5OH, a reduction and oxidation mechanism with nitric oxide (NO), adsorption and desorption of C_2H_5OH on zeolites and oxidation of CH_3CHO. The experimental work carried out included light-off performance tests where the conversion performance of the catalyst was measured. The kinetic parameters extracted from experimental data were presented and incorporated within a two-dimensional catalyst model.

Due to the oxygen rich nature of the gas feeds used by Stepanek et al., the kinetic parameters are not applicable to a TWC fitted to a SI engine using ethanol containing fuel. There is a lack of available data regarding the behaviour and simulation of a TWC exposed to stoichiometric ethanol-fuelled engine exhaust gas species.

The work reported in this paper focuses on clarifying the chemical reaction pathways for a TWC exposed to ethanol-fuelled engine exhaust gas species, and defining the promoting and inhibiting species for each key reaction to allow the definition of kinetic rate equations.

2. Experimental Setup

The catalyst samples were supplied by Jaguar Land Rover (JLR)and had a precious metal loading of 150 g ft^{-3} or 50 g ft^{-3} (Pd and Rh in a ratio of 29:1 in both cases) and 600 cpsi cell density. Cores of 30mm diameter and 75mm length were removed from a full sized brick for analysis.

A synthetic gas reactor (Horiba SIGU 2000) was used to assess the performance of the catalyst samples. This reactor allows both gas and liquid HCs to be introduced to the gas mixture and also has the ability to simulate closed loop air-fuel ratio (AFR) perturbation in an SI engine via separate perturbation mass flow controllers. The sample outlet gases were analysed using a Horiba 6000FT FTIR analyser for HC speciation, and a Horiba MEXA 7170 (CO, CO_2, O_2, THC and NO_x). Further details on the experimental equipment used in this study are available in McAtee *et al.* (18).

A typical temperature profile for activity testing is reported in Figure 1. The procedure of using a warm up temperature ramp followed by two subsequent measurement temperature ramps was established in previous work to ensure that the catalyst surface is in the same condition prior to each test (19), thereby improving the repeatability of the measurements.

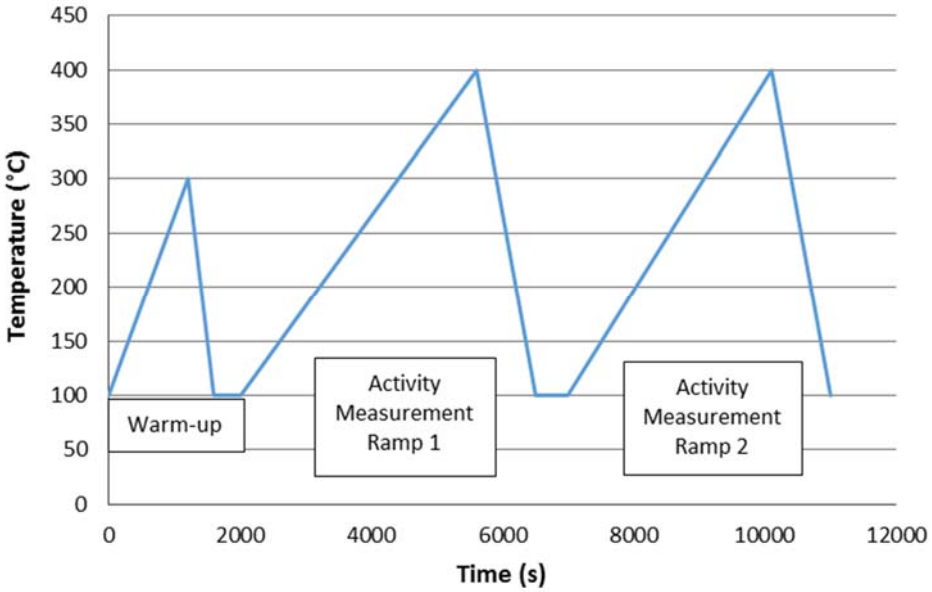

Figure 1 Temperature Profile for Activity Testing

The tests conducted included individual performance tests for C_2H_5OH, CH_3CHO, C_3H_6, C_3H_8 and CO. Following this, each HC was tested in the presence of CO on the basis that CO typically has a strong inhibiting effect on HC oxidation. All tests were performed at stoichiometric O_2 conditions and the O_2 concentration was calculated accordingly for each test. All tests were performed at a space velocity of 50,000 h^{-1}. Finally, a full gas mixture was

tested which also included NO and CH_4. The concentrations of each gas are shown in Table 1. In all cases nitrogen (N_2) was used as the balance gas.

Table 1 Gas Component Concentrations for Individual and Mixture Tests

Gas Component	Concentration
C_2H_5OH	300ppm
CH_3CHO	100ppm
C_3H_6	150ppm
C_3H_8	100ppm
CO	0.5%
NO	400ppm
CH_4	150ppm
CO_2	12%
H_2O	5%

In addition to the activity tests performed using the synthetic gas reactor, the thickness of the channel wall and the washcoat were measured for modelling purposes using a JOEL 6500 scanning electron microscope.

3. Experimental Results

3.1 Ethanol-Oxygen Variation Tests

The impact of O_2 on the dehydrogenation, decomposition and oxidation of C_2H_5OH was assessed at three stoichiometric ratios as shown in Table 2. The O_2 concentrations were calculated on a stoichiometric basis i.e. a C_2H_5OH:O_2 molar ratio of 1:3 was required to achieve full conversion.

Table 2 C_2H_5OH and O_2 Variation Tests

C_2H_5OH Concentration	O_2 : C_2H_5OH	O_2 Concentration (vol.%)

(ppm)	Stoichiometric Ratio	
150	0.6, 1.0, 1.5	0.027, 0.045, 0.068
300	0.6, 1.0, 1.5	0.054, 0.090, 0.135
1000	0.6, 1.0, 1.5	0.180, 0.300, 0.450

The first step in ethanol conversion was expected to be the formation of CH_3CHO, the experimental results of which are in Figure 2. For all three ethanol concentrations explored, an increase in CH_3CHO concentration was observed until about a third of the inlet C_2H_5OH was converted, which typically occurred at 150 - 175°C. In all cases the O_2 : C_2H_5OH ratio had little to no impact on the reaction profile which suggests that CH_3CHO is predominantly formed via dehydrogenation, rather than the partial oxidation, of C_2H_5OH.

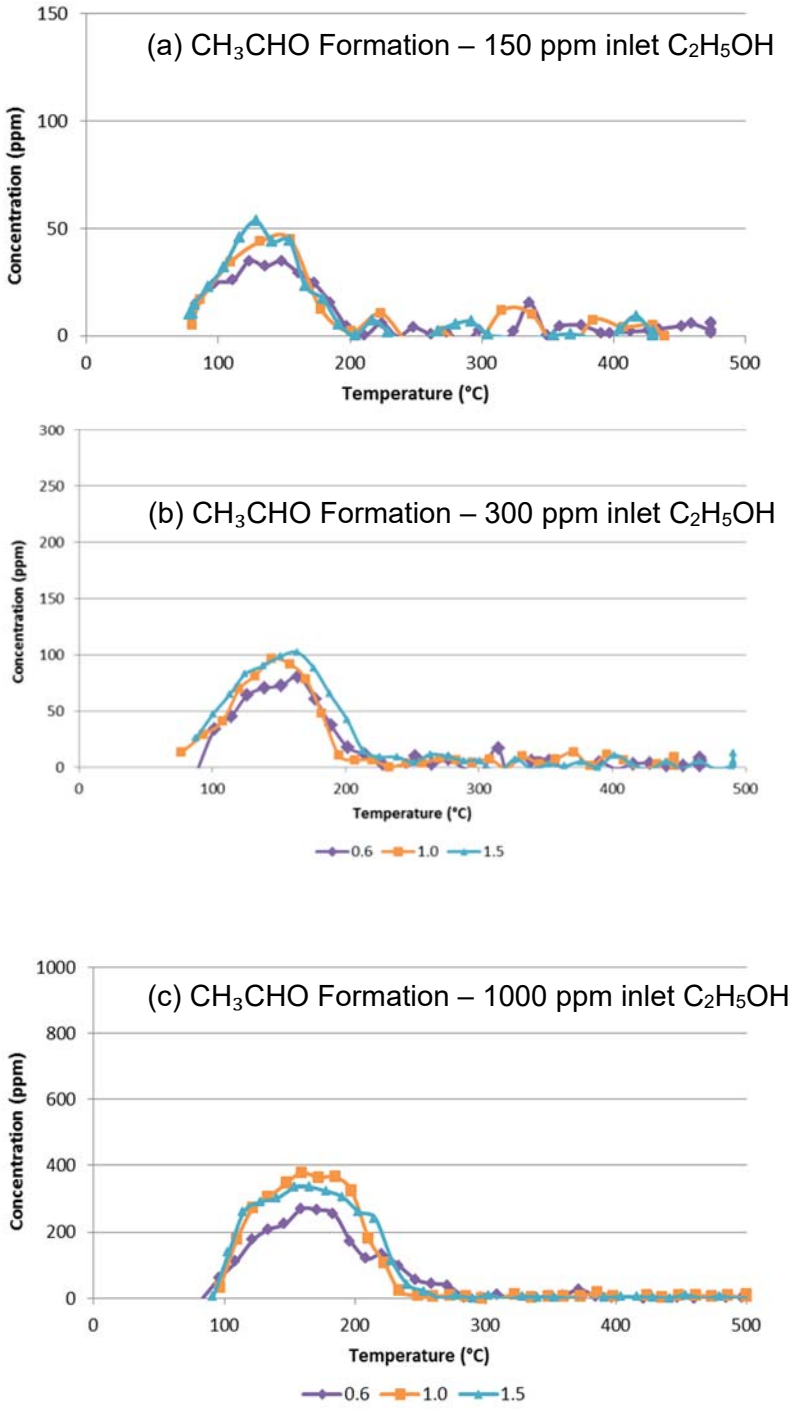

Figure 2 CH_3CHO Formation from a) 150ppm, b) 300ppm, c) 1000ppm C_2H_5OH Inlet at Stoichiometric Ratios of 0.6, 1.0 and 1.5

Evolution of CH_4 was also observed, which is reported in Figures 3 to 5. A peak CH_4-make of 50ppm was observed at all stoichiometric ratios when 150ppm of ethanol was fed (Figure 3) to the catalyst, meaning that approximately two thirds of the inlet C_2H_5OH was converted

to CH_3CHO and CH_4. When the oxygen concentration was decreased (i.e. ratio of 0.6), CO was evolved coupled with sustained CH_4 generation at higher temperatures.

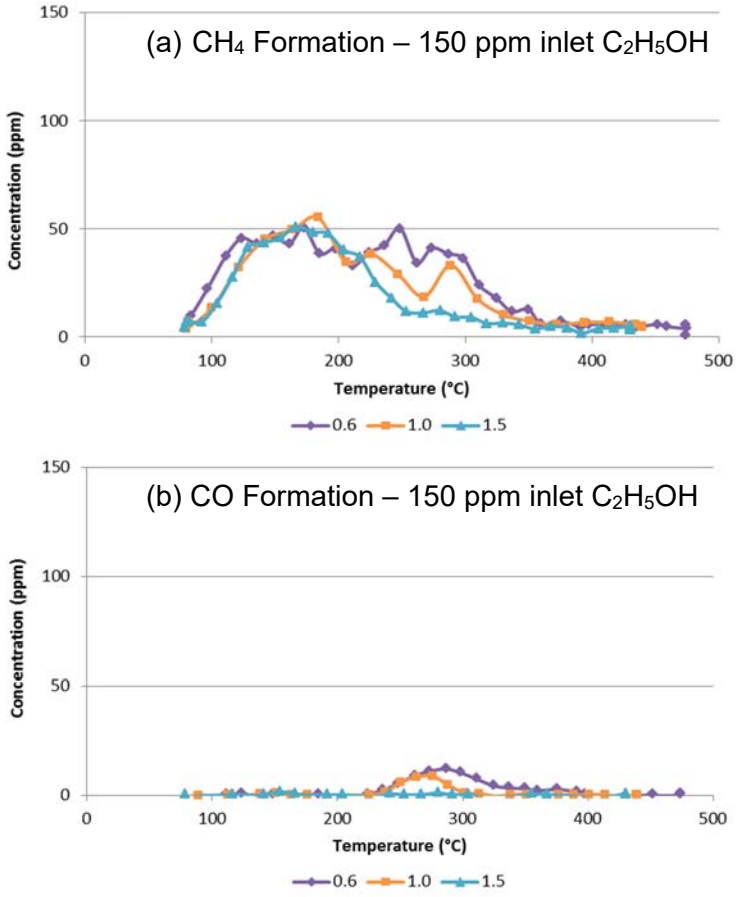

Figure 3 Formation Trends for a) CH_4 and b) CO with 150ppm C_2H_5OH Inlet at Stoichiometric Ratios of 0.6, 1.0 and 1.5

Doubling the ethanol feedgas concentration to 300 ppm (Figure 4) led to a similar trend (i.e. CH_4 and CO evolution at low oxygen conditions). Increasing the ethanol concentration to 1000ppm (Figure 5) further illustrates the formation of CH_4 and CO via the decomposition of CH_3CHO (Eq. 2). A key feature of these results is that significant quantities of CH_4 and CO remain unreacted at temperatures in the range 300 – 500 °C when the stoichiometric ratio is set at 0.6. The reason for this trend is that, while temperature of the catalyst is sufficient to promote oxidation of CH_4 and CO, there is insufficient oxygen in the feed gas to permit both of these reactions to proceed to completion.

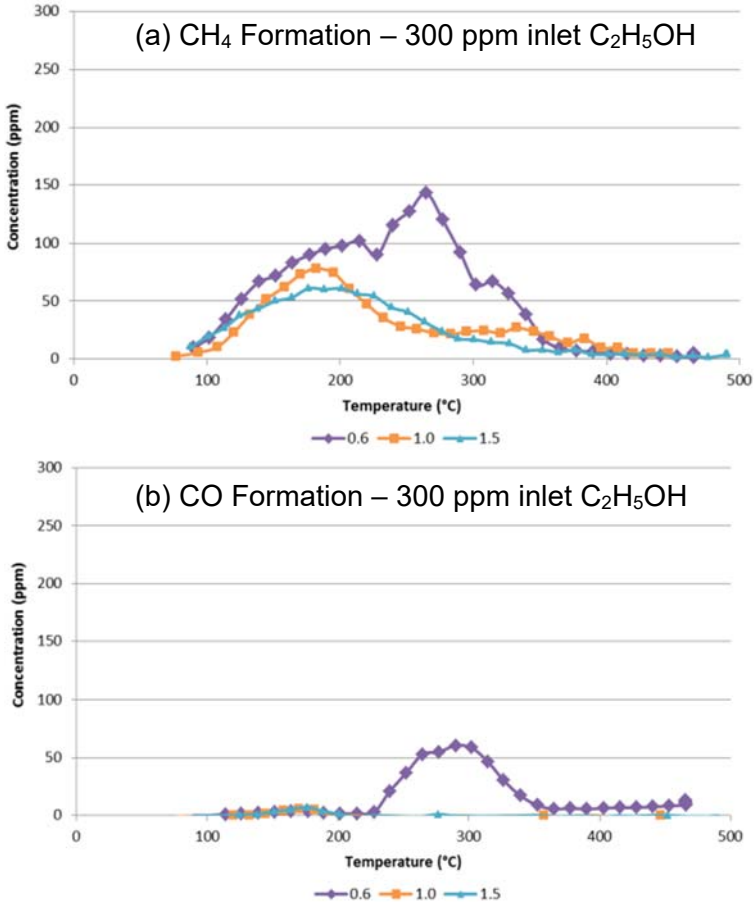

Figure 4 Formation Trends for a) CH_4 and b) CO with 300ppm C_2H_5OH Inlet at Stoichiometric Ratios of 0.6, 1.0 and 1.5

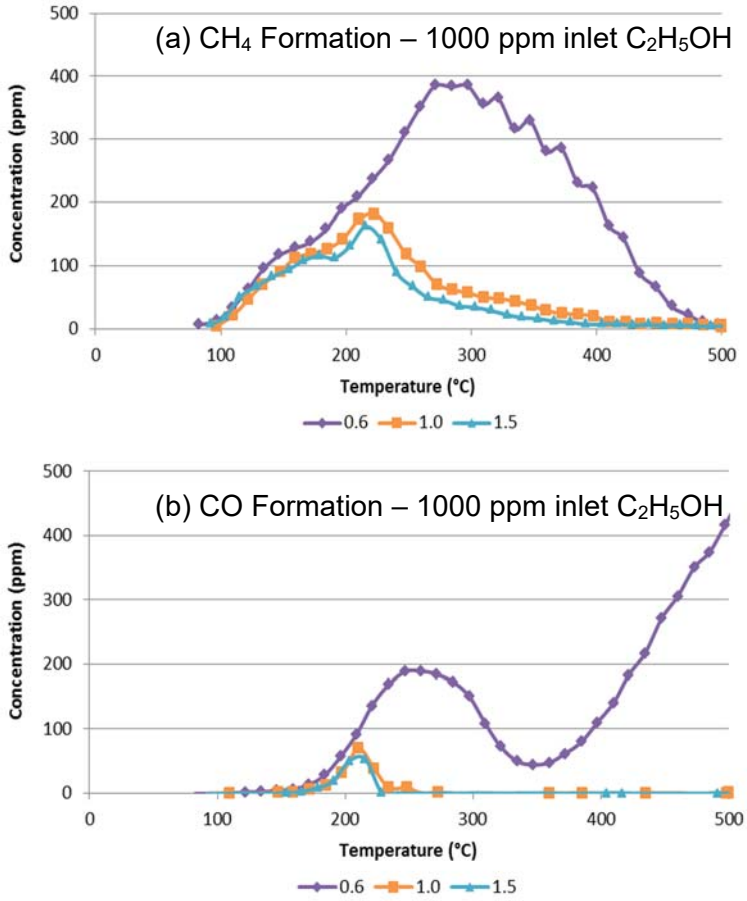

Figure 5 Formation Trends for a) CH_4 and b) CO with 1000ppm C_2H_5OH Inlet at Stoichiometric Ratios of 0.6, 1.0 and 1.5

3.2 Inhibition factors to ethanol conversion

To construct the kinetic equations for each of the reactions involving C_2H_5OH it was necessary to understand the interactions between each compound. Using the component concentrations given in Table 1, the conversion of C_2H_5OH in the presence of the other compounds separately was probed. The only significant inhibitors to C_2H_5OH conversion were found to be CO and NO, which is consistent with the findings of previous studies of hydrocarbon reaction kinetics (17). To investigate their effect in greater detail, the tests were repeated at different CO (0.5, 1 and 1.5 vol %) and NO (400, 1000 and 1500 ppm) concentrations.

3.3 The inhibition effect of CO

Figure 6 shows that only a relatively low concentration of CO is required to produce an inhibiting effect for both C_2H_5OH and THC conversion. The role of CO can be explained further by examining the formation trends for CH_3CHO and CH_4 as reported in Figure 7. The presence of CO resulted in greater CH_3CHO formation and shifted the generation of CH_4 to higher temperatures, confirming that the presence of CO has an inhibiting effect on the decomposition of CH_3CHO to form CH_4. Moreover, the fact that the formation of CH_4 continued to a higher temperature in the presence of CO indicated that it also inhibited CH_3CHO oxidation. These results also showed that CO does not significantly inhibit C_2H_5OH dehydrogenation and hence can be omitted from its kinetic rate equation.

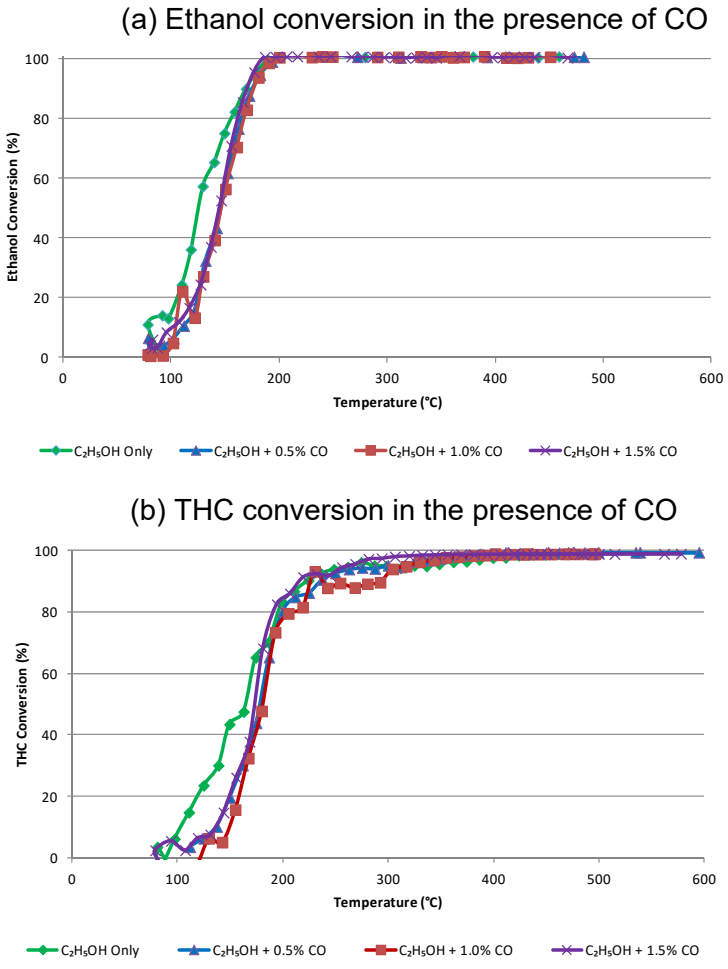

Figure 6 C_2H_5OH (a) and THC (b) Conversions in the Presence of Varying Concentrations of CO

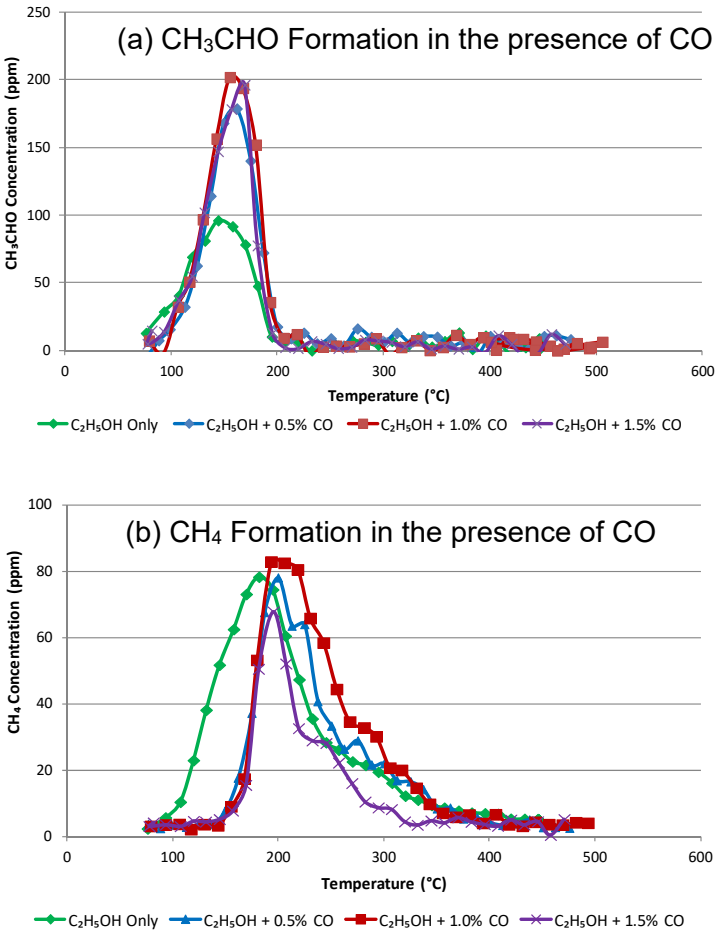

Figure 7 CH_3CHO (a) and CH_4 (b) Formation in the Presence of Varying Concentrations of CO

3.4 The inhibition effect of NO

The presence of NO did not significantly affect the dehydrogenation of C_2H_5OH as shown by the conversion efficiency graphs in Figure 8. While a small increase in light-off temperature was evident when 400ppm NO was added to the feed gas, increasing the NO concentration to 1500ppm had no additional impact on this reaction. Peak C_2H_5OH conversion efficiency was also unaffected by the presence of NO, regardless of its concentration. However, the presence of NO did inhibit the subsequent decomposition of CH_3CHO and formation of CH_4, seen in Figures 9(a) and 9(b) respectively. While the temperature at which CH_3CHO formed, 100-150 ^oC in Figure 9 (a), was unaffected by NO, the temperature at which it decomposed increased as NO was added to the feed gas. This trend is confirmed by the formation of CH_4 seen in Figure 9(b), which

occurred at increasing temperatures as the concentration of NO was increased. The temperature at which CH_4 oxidised also increased in the presence of NO.

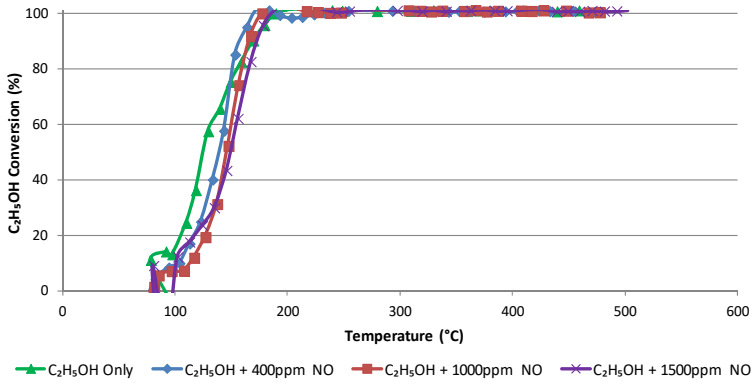

Figure 8 C_2H_5OH Conversion Curves in the Presence of Varying Concentrations of NO

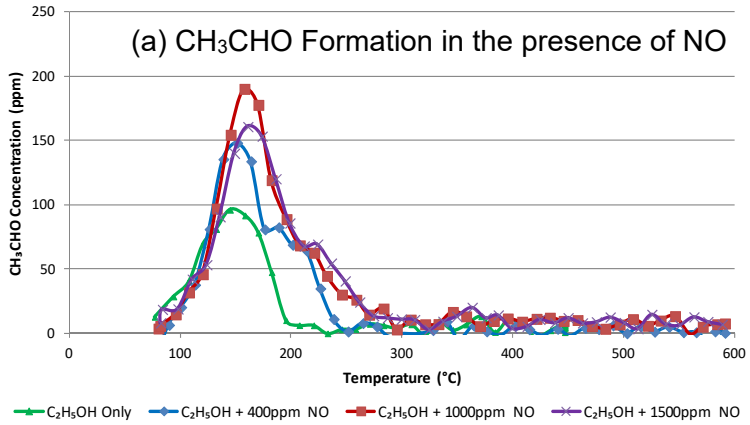

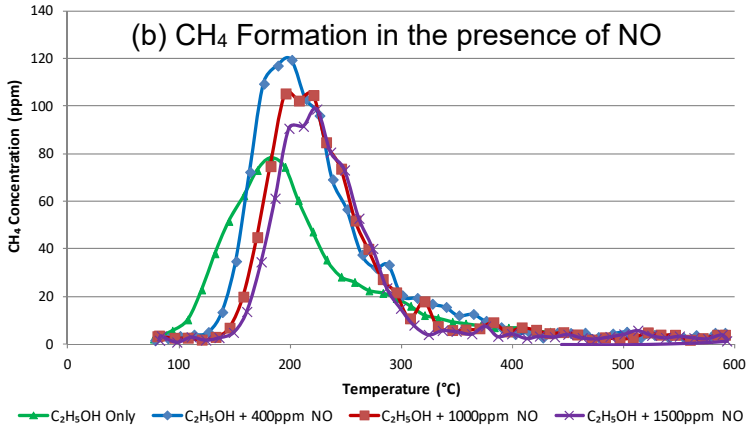

Figure 9 CH_3CHO (a) and CH_4 (b) formation curves in the Presence of Varying Concentrations of NO

3.5 Summary of catalyst characterisation

The effects of the reactants and products on the C_2H_5OH and CH_3CHO reactions were:

- C_2H_5OH dehydrogenation to form CH_3CHO is little affected by CO or NO.
- CO and NO inhibit both CH_3CHO decomposition and CH_3CHO oxidation.
- There is no inhibiting effect for CH_3CHO, C_3H_8, C_3H_6 and CH_4.

Based on the above results, the general pathway for conversion of C_2H_5OH over this PdRh catalyst is believed to be;

1. C_2H_5OH dehydrogenation forming CH_3CHO
2. CH_3CHO decomposition to form CH_4 and CO at low temperatures (below ~ 200 °C)
3. when the catalyst temperature is sufficiently high, the majority of the CH_3CHO is fully oxidised. Due to the observation of prolonged formation of CH_4, it is reasonable to conclude that the decomposition of CH_3CHO continues alongside CH_3CHO oxidation.

It is difficult to draw conclusions on the direct full oxidation of C_2H_5OH; if it occurs at a temperature higher than that of the CH_3CHO oxidation then its evaluation would be challenging. Consequently, a kinetic equation is included for the full oxidation of C_2H_5OH for modelling purposes with the assumption that the reaction is inhibited by CO and NO.

4. Formulation of Kinetic Equations

The model used to simulate the behaviour of the catalyst sample was Axisuite by Exothermia (20). This commercially available software is used by the sponsoring company to model various catalyst formulations and so it was the preferred choice of simulation tool in which to add the new reactions. The Axicat module of Axisuite was used in this study as the

sample under investigation was a flow-through TWC. The module requires catalyst specification data including precious metal loading and geometric dimensions. The inlet gas concentrations, which are specified by the user, can be constant as required for synthetic gas reactor testing, or derived from transient drive cycle emissions data taken from on-engine tests. Temperature profile and mass flow rate data are also essential requirements. The module requires catalyst specification data including precious metal loading, geometric dimensions and cell density. C_2H_5OH and CH_3CHO are not included in the standard gas species configuration of Axisuite and, at the authors' request, these were added by Exothermia to a specially devised reaction scheme. This allowed for implementation of the required C_2H_5OH and CH_3CHO reactions and kinetic parameters. The structures of the standard kinetic equations in Axicat are based on the standard Langmuir-Hinshelwood expressions traditionally used to represent the surface reaction rates within catalysts (16, 17). These expressions include the promotional and inhibiting compounds and their respective kinetic coefficients for each reaction. Axisuite contains 35 pre-programmed inhibition parameters. Ten additional inhibition rate values were added to this standard list in order to incorporate the requirements of the new C_2H_5OH and CH_3CHO reactions. This provided maximum flexibility with respect to derivation of the coefficient values for each new reaction. The sequence of reactions proposed from the experimental work are summarised in Table 3, and are described in Equations 4 – 7.

To achieve acceptable agreement between experimental and theoretical temperature predictions at catalyst sample exit, the heat transfer coefficients were tuned until good agreement with the SIGU 2000 synthetic gas generator temperature profile was achieved. The parameters modified to achieve this were the canning density, canning thermal capacity, insulation thermal conductivity and density.

Table 3 Summary of Reactions and Reaction Sequence

Step no.	Description	Reaction	Eq.
1	Ethanol dehydrogenation	$C_2H_5OH \rightarrow CH_3CHO + H_2$	4
2	Acetaldehyde decomposition	$CH_3CHO \rightarrow CH_4 + CO$	5
3	Acetaldehyde oxidation	$CH_3CHO + 2.5O_2 \rightarrow 2CO_2 + 2H_2O$	6
4	Ethanol oxidation	$C_2H_5OH + 3O_2 \rightarrow 2CO_2 + 3H_2O$	7

The kinetic equation for ethanol dehydrogenation, Equation 8, is relatively simple as the other compounds in the feed gas do not introduce an inhibiting effect.

$$r_{C_2H_5OH_{dehydro}} = \frac{k^r{}_{C_2H_5OHdehydro}[C_2H_5OH]}{(1 + k^{inh}_{C_2H_5OH\_1}[C_2H_5OH])} \quad \text{Eq. 8}$$

The C_2H_5OH inhibition term refers to C_2H_5OH's self-inhibition and in this case it is the only inhibiting factor.

CO and NO inhibit CH_3CHO decomposition, and as per the previous equation, a CH_3CHO self-inhibition term is also required as shown in Equation 9.

$$r_{CH_3CHO\ dec} = \frac{k^r{}_{CH_3CHOdec}[CH_3CHO]}{(1 + k^{inh}_{CO\_1}[CO])(1 + k^{inh}_{NO\_1}[NO])(1 + k^{inh}_{CH_3CHO\_1}[CH_3CHO])} \quad \text{Eq. 9}$$

CO and NO inhibit CH_3CHO oxidation, whereas CH_3CHO and O_2 promote it. Allowance for these effects is made in Equation 10.

$$r_{CH_3CHO\ ox} = \frac{k^r{}_{CH_3CHOox}[CH_3CHO][O_2]}{(1 + k^{inh}_{CO\_2}[CO])(1 + k^{inh}_{NO\_2}[NO])(1 + k^{inh}_{CH_3CHO\_2}[CH_3CHO])} \quad \text{Eq. 10}$$

The definition of the C_2H_5OH oxidation kinetic equation is more challenging as it was not possible to observe the direct oxidation of C_2H_5OH from the experimental data. However, including an expression allows for flexibility with respect to simulation work. It is assumed that the inhibitors of C_2H_5OH oxidation would be CO and NO as shown in Equation 11.

$$r_{C_2H_5OH\ ox} = \frac{k^r{}_{C_2H_5OHox}[C_2H_5OH][O_2]}{(1 + k^{inh}_{CO\_3}[CO])(1 + k^{inh}_{NO\_3}[NO])(1 + k^{inh}_{C_2H_5OH\_2}[C_2H_5OH])} \quad \text{Eq. 11}$$

The repetition of gas species in various inhibition functions was introduced to allow maximum flexibility in the investigation of the pre-exponential and activation energy coefficients for each reaction. This approach allowed assessment of the effect of each inhibition function on individual reactions. This is particularly helpful where chain-reactions occur such as CH_3CHO decomposition which is heavily dependent on the preceding C_2H_5OH dehydrogenation reaction.

Note that both rate constants and inhibition coefficients are represented using an Arrhenius dependence as described in Equation 12.

$$k_i = Ae^{\left(\frac{E_a}{RT}\right)} \quad i = species \qquad \text{Eq. 12}$$

5. Kinetic Parameter Optimisation

5.1 Single Component Test Simulation

The kinetic expressions defined in Section 4 were fed into the reaction schemes of Exothermia's Axisuite after-treatment modelling package. Initially, the C_2H_5OH only tests (150, 300, 1000 ppm concentrations) were simulated to produce the promoting kinetic coefficients for C_2H_5OH dehydrogenation and oxidation, CH_3CHO decomposition and oxidation without the inhibition of compounds such as CO and NO. Additionally, the self-inhibition kinetic coefficients were required, specifically $k^{inh}_{C_2H_5OH\_1}$ (C_2H_5OH self-inhibition) for C_2H_5OH dehydrogenation, $k^{inh}_{CH_3CHO\_1}$ (CH_3CHO self-inhibition) for CH_3CHO decomposition, $k^{inh}_{C_2H_5OH\_2}$ (C_2H_5OH self-inhibition) for C_2H_5OH oxidation and $k^{inh}_{CH_3CHO\_2}$ (CH_3CHO self-inhibition) for CH_3CHO oxidation. As previously stated some repetition of gas species with different kinetic coefficients occur to allow for maximum flexibility i.e. one kinetic coefficient affects only one reaction. It should be noted that it was the goal of the authors to achieve consistency of coefficients for each gas species. For example, $k^{inh}_{CH_3CHO\_1}$ and $k^{inh}_{CH_3CHO\_2}$

would consist of the same pre-exponential and activation energy values as they both refer to the self-inhibition of CH_3CHO.

The determination of the kinetics parameters was achieved through a manual iterative process. Once each simulation had been matched, a process of convergence was undertaken in order to identify trends in the coefficients and eventually converge on a set of coefficients which produced acceptable correlation across the set of simulated and measured data. The process began with the initial estimation of C_2H_5OH dehydrogenation kinetic coefficient values for the 300ppm C_2H_5OH only test, which was then compared with those values obtained for the 1000ppm C_2H_5OH only simulation.

To determine the pre-exponential and activation energy values for the C_2H_5OH dehydrogenation reaction an estimation was made whilst the coefficients for subsequent reactions were set to zero. Although the rate of disappearance of C_2H_5OH and the concentration of CH_3CHO are also affected by the subsequent CH_3CHO decomposition reaction, this approach was the least complex method of making an initial estimation of the dehydrogenation coefficients. This prediction was then compared to the measured data and the kinetic parameters adjusted iteratively to minimise the error between the two. This process was repeated for CH_3CHO formation and then CH_4 formation. This sequence was repeated until kinetic parameters for all three reactions simultaneously produced simulated data that matched the measured data. After some alteration of the kinetic coefficients, a good correlation was achieved for each of the concentration traces as shown in Figure 10. Other kinetic parameters involved in reactions such as the oxidation of CO, CH_4, C_3H_6 and C_3H_8 were kept at the default values and so only the values of the new kinetic terms are reported here.

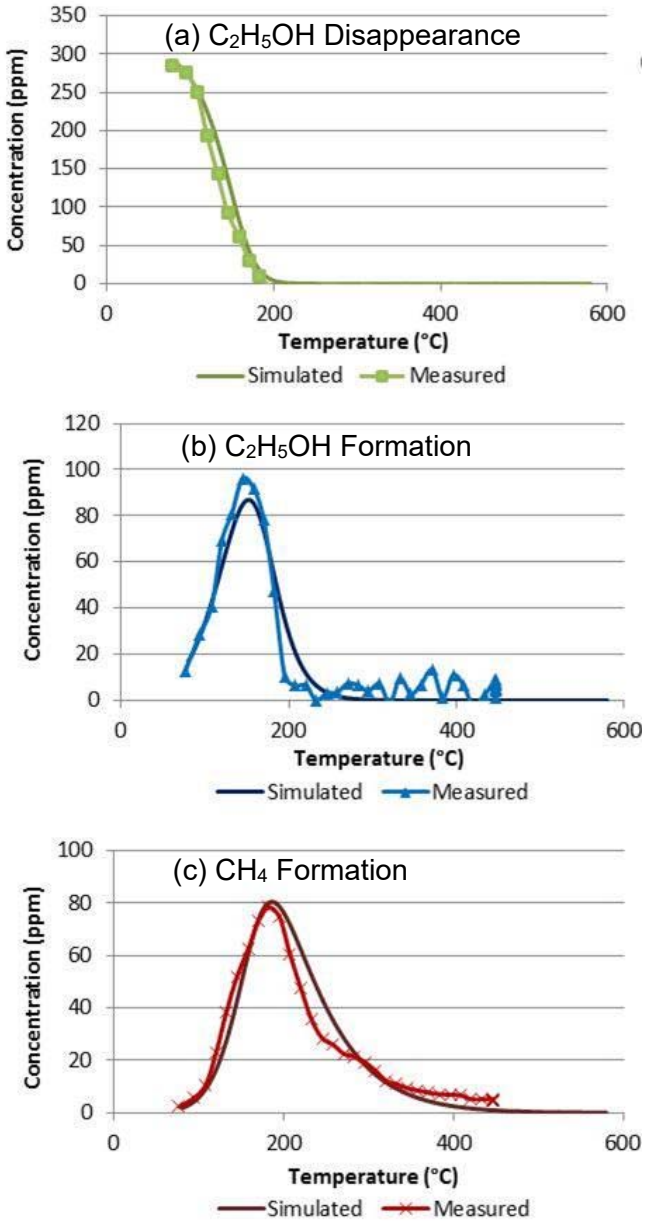

Figure 10 C_2H_5OH Oxidation Reaction Activated. 300 ppm C_2H_5OH in feed gas. A = 3.5 x 10^{20} s^{-1} Ea = 101,000 J mol^{-1}

The simulation and experimental results were not an exact match (as expected) as self-inhibition was not included at this stage. The values of the kinetic parameters obtained during this phase of the process are summarised in Table 4.

The coefficients established in the 300ppm simulation were then used for the 1000ppm simulation to assess the output in comparison with its corresponding experimental results as shown in Figure 11.

Table 4 Promotional Kinetic Coefficients Estbalished from 300ppm Ethanol Test

Reaction	**k^{0r} (s^{-1} or m^3 mol^{-1} s^{-1})**	**E^r (J mol^{-1})**
C_2H_5OH Dehydrogenation	4.0×10^9	35,000
C_2H_5OH Oxidation	3.5×10^{20}	101,000
CH_3CHO Decomposition	9.0×10^8	29,000
CH_3CHO Oxidation	3.0×10^{18}	92,000

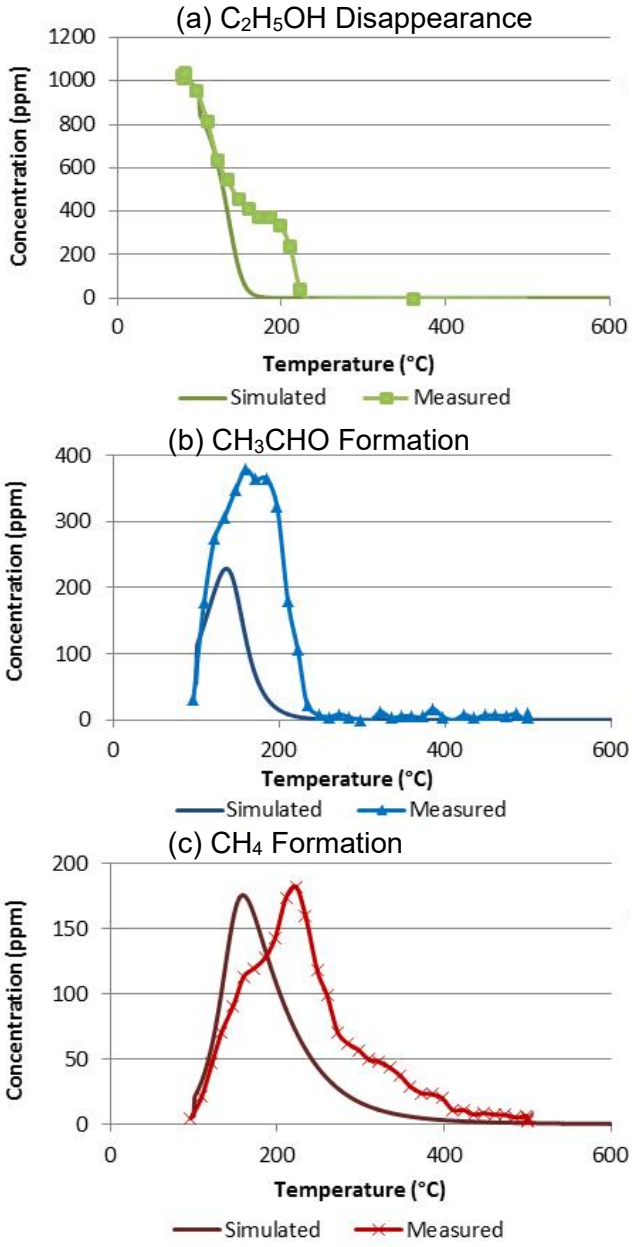

Figure 11 1000ppm C_2H_5OH Simulated and Measured Results using 300ppm Derived Coefficients

It was clear that the coefficients established using the 300ppm C_2H_5OH data were not directly transferable to the 1000ppm test which highlighted the need for self- and cross-inhibition terms to be included.

Temperature differences between the simulated and measured data for CH_3CHO and CH_4 formation were observed. For example the disappearance of CH_3CHO and the peak formation of CH_4 in the simulated data occur at a lower temperature than observed

experimentally (Figure 11 b and c). This is caused by the absence of CH_3CHO self-inhibition which is required in its decomposition as well as oxidation reactions. Additionally, when considering tests which incorporate other compounds such as CO and NO, further alteration was required to take their inhibiting effects into account.

Using data reported in literature as a starting point for the inhibition coefficients (12,13), an optimization of the parameters through an iterative process was carried out using the C_2H_5OH + CO, C_2H_5OH + NO and C_2H_5OH only data as objective functions. A set of values was established that provided the most agreeable compromise with respect to the difference between simulated and measured data. An example of the quality of the match between the experimental data and the simulation is reported in Figure 12 for the case 300ppm C_2H_5OH only experiments.

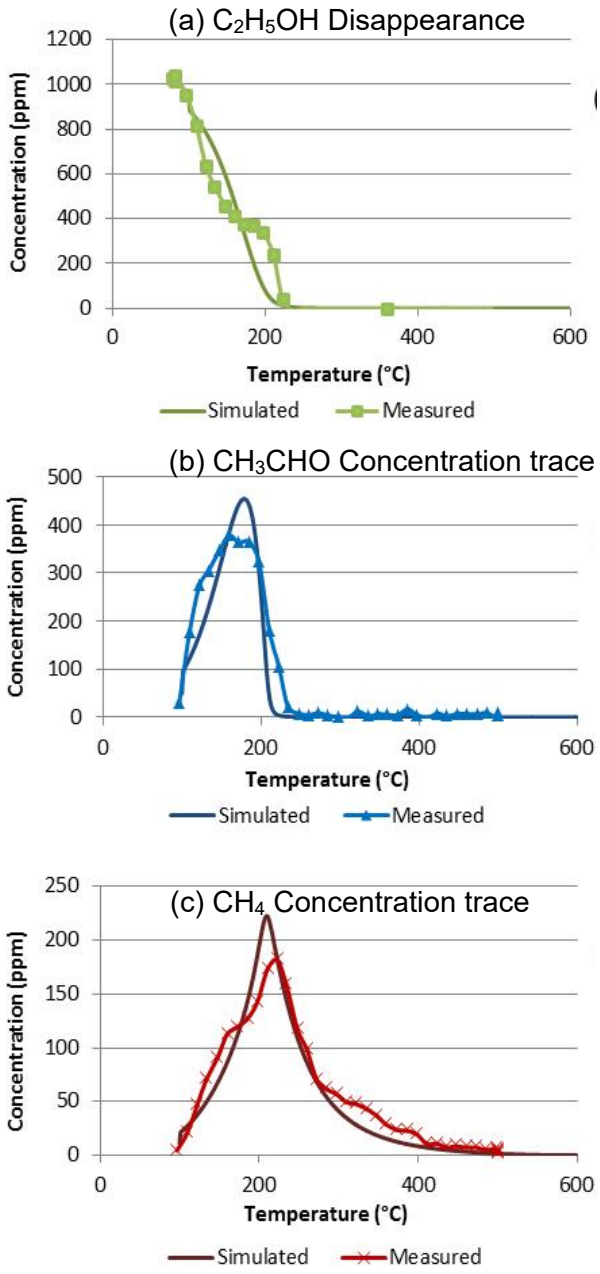

Figure 12 1000ppm C_2H_5OH Only Test Simulated and Measured Data using 300ppm Derived Coefficients and new Inhibition Coefficients

5.2 Full Mixture Test Simulation

The full mixture test was used to refine the kinetic coefficients obtained thus far, based on their best fits between overall simulation performance and the range of experimental tests (Tables 5 and 6).

Table 5 Final Kinetic Promotional Coefficients

Reaction	**k^{0r} (s^{-1} or m^3 mol^{-1} s^{-1})**	**E^r (J mol^{-1})**
C_2H_5OH dehydrogenation	3.6 x 10^{11}	48,500
CH_3CHO decomposition	1.4 x 10^9	25,200
CH_3CHO oxidation	5.65 x 10^{18}	84,400
C_2H_5OH oxidation	9.5 x 10^{18}	108,000

Table 6 Final Kinetic Inhibition Coefficients

Inhibition Parameter and Corresponding Gas Species			**k^{0inh} (m^3 mol^{-1})**	**E^{inh} (J mol^{-1})**
C_2H_5OH dehydrogenation	Self-inhibition	$k^{inh}_{C_2H_5OH\_1}$	4.1 x 10^2	-2460
CH_3CHO decomposition	Self-inhibition	$k^{inh}_{CH_3CHO\_1}$	6.8 x 10^3	-6950
	Inhibition by CO	$k^{inh}_{CO\_1}$	65.5	-7990
	Inhibition by NO	$k^{inh}_{NO\_1}$	1.9 x 10^2	-17150
CH_3CHO oxidation	Self-inhibition	$k^{inh}_{CH_3CHO\_2}$	6.8 x 10^3	-6950
	Inhibition by CO	$k^{inh}_{CO\_2}$	65.5	-7990
	Inhibition by NO	$k^{inh}_{NO\_2}$	4.79 x 10^5	31036
C_2H_5OH oxidation	Self-inhibition	$k^{inh}_{C_2H_5OH\_2}$	4.1 x 10^2	-2460
	Inhibition by CO	$k^{inh}_{CO\_3}$	65.5	-7990
	Inhibition by NO	$k^{inh}_{NO\_3}$	4.79 x 10^5	31036

The result of using these parameters in the full ethanol mix test show good correlation between the simulated and measured data (Figures 13-16).

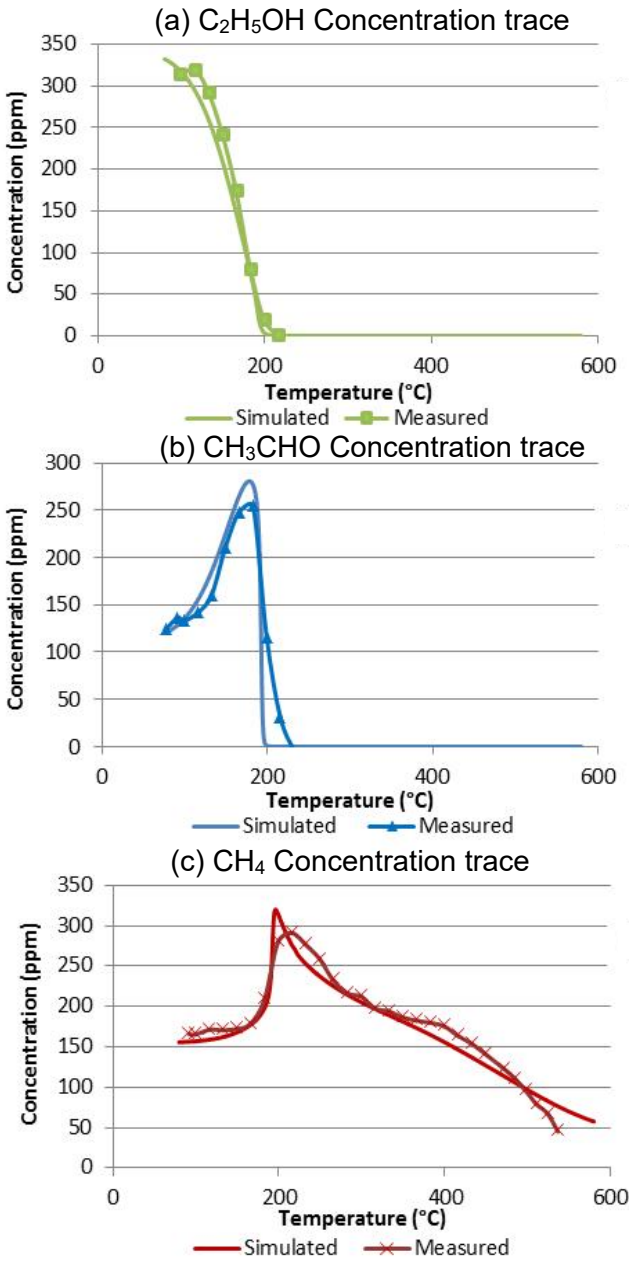

Figure 13 Concentration Traces from Full E85 Exhaust Mixture Simulation and Measured

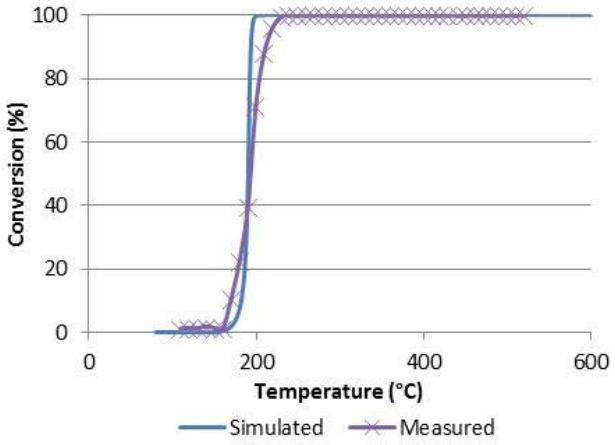

Figure 14 CO Conversion Simulated and Measured, Full Mixture

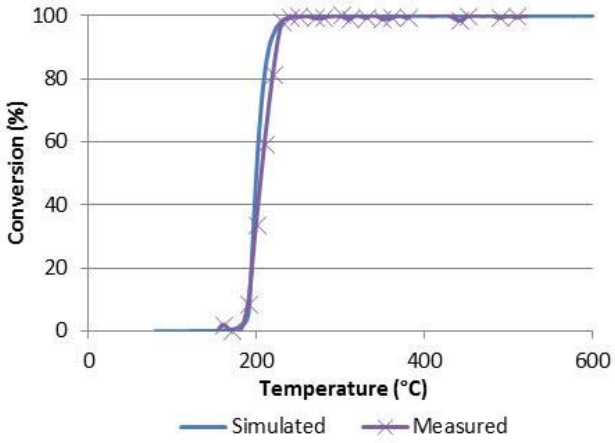

Figure 15 C_3H_6 Simulated and Measured, Full Mixture

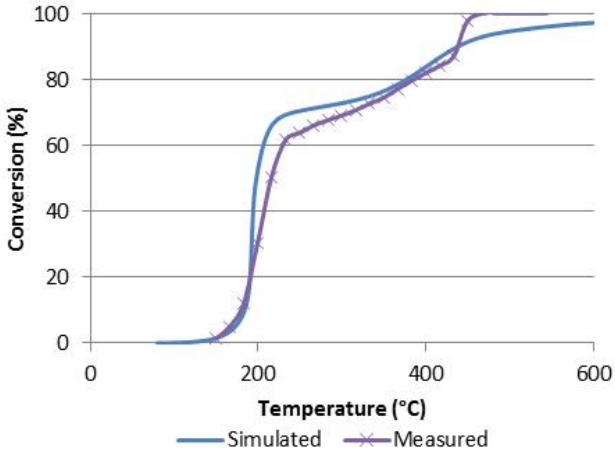

Figure 16 THC Simulated and Measured, Full Mixture

6. Model Validation using 50 g/ft^3 PdRh catalyst

A final model validation using an identical PdRh automotive catalyst, with the exception of the overall precious metal loading being reduced to 50g ft^{-3}, was carried out in order to confirm that the reaction pathways derived using the 150 g ft^{-3} sample could be transferred.

The experimental results and simulations are reported in Figures 17 to 20. The disappearance of C_2H_5OH in the simulation is predicted at a slightly lower temperature than measured and is a result of CH_3CHO formation and subsequent decomposition (Figure 17). The disappearance of CH_3CHO is also simulated to start at a lower temperature than measured which appears to be due to excessive CH_4 formation and full oxidation. As a result, the onset of the THC conversion (Figure 20) is predicted to occur at a lower temperature than what was measured; the high temperature (>250°C) conversion corresponds with the CH_4 conversion behaviour observed over the same temperature range. The prediction of the CO, C_3H_6 and THC conversions, shown in Figures 18-20 respectively, are also in good agreement with the measured data. Considering that no attempt was made at further tuning the parameters defined using the 150 g ft^{-3} sample, the correspondence between the experimental data and the simulated results is remarkable.

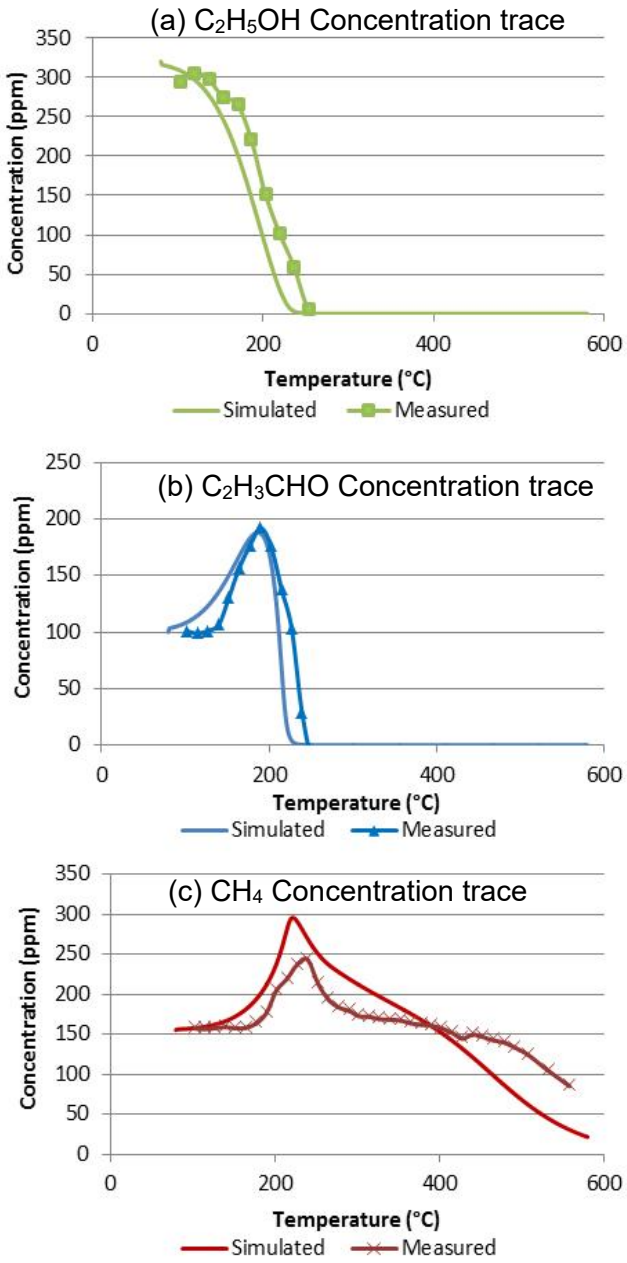

Figure 17 50g/ft^3 PdRh Sample Full Mixture Simulated and Measured Comparison

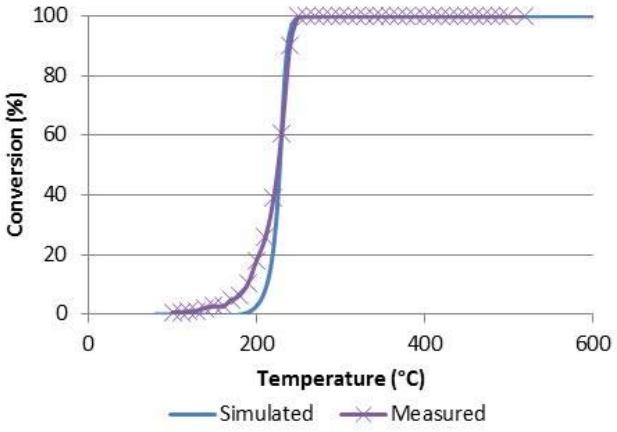

Figure 18 50g/ft³ CO Conversion Simulated and Measured Comparison

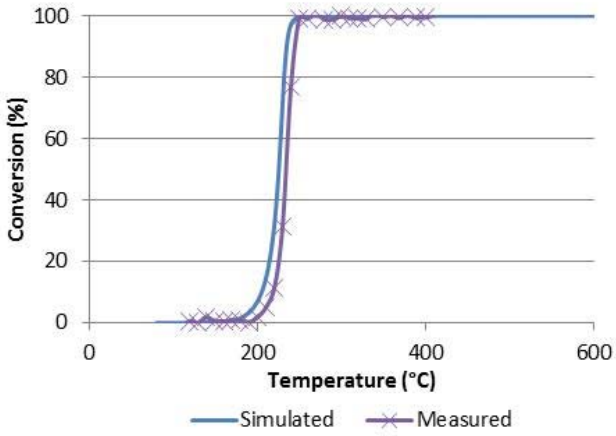

Figure 19 50g/ft³ C_3H_6 Conversion Simulated and Measured Comparison

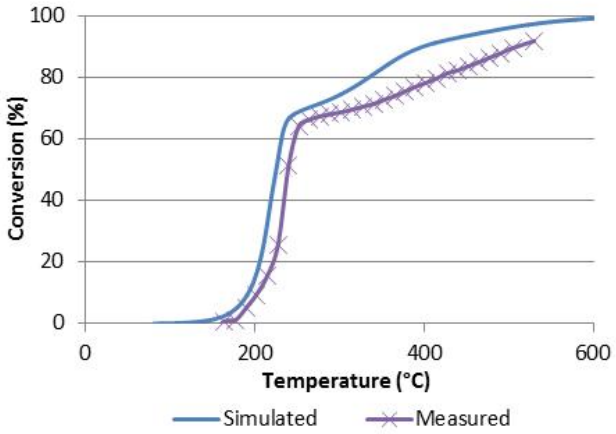

Figure 20 50g/ft³ THC Conversion Simulated and Measured Comparison

7. Conclusions

The performance of a PdRh automotive catalyst was evaluated when subjected to a range of concentrations of C_2H_5OH and CH_3CHO at varying stoichiometric ratios, and the effect of O_2 concentration on the dehydrogenation and decomposition reactions was clarified. The inhibiting compounds to these reactions were determined along with the effect of their concentrations. Analysis of CH_3CHO formation using various C_2H_5OH inlet concentrations and stoichiometric ratios showed that:

- C_2H_5OH dehydrogenation is independent of O_2 concentration
- CO and NO were found to be the main inhibiting compounds to CH_3CHO decomposition, CH_3CHO oxidation and C_2H_5OH oxidation.
- C_2H_5OH dehydrogenation was not significantly affected by the presence of CO or NO.

The experimental work provided a suitable structure for the derivation of the kinetic equations required to develop a simulation of the reactions. An iterative manual optimization process was used to derive a set of global kinetics parameters representative of the catalyst performance when exposed to exhaust gas from E85-fuelled SI engine. The kinetic parameters were validated by using a lower loading PdRh catalyst, which showed remarkably good correlation, confirming that the model can be used to describe the behaviour of PdRh catalysts when exposed to E85 exhaust effluents. It is particularly noteworthy that the formation of CH_4 via the decomposition of CH_3CHO results in full conversion of THC being delayed until the catalyst inlet temperature reaches approximately 600 ^oC.

Nomenclature

Symbols

A	Pre-exponential frequency factor	s^{-1}
E_a	Activation energy	J mol^{-1}
i	Gas species	
$k^{0\,inh}$	Inhibition rate constant	m^3 mol^{-1}
$k^{0\,r}$	Promotional rate constant	m^3 mol^{-1}
$k^r{}_{C_2H_5OHdehydro}$	C_2H_5OH promotional coefficient dehydrogenation	s^{-1}
$k^r{}_{C_2H_5OHox}$	C_2H_5OH promotional coefficient oxidation	m^3 mol^{-1} s^{-1}
$k^r{}_{CH_3CHOdec}$	CH_3CHO promotional coefficient decomposition	s^{-1}
$k^r{}_{CH_3CHOox}$	CH_3CHO promotional coefficient oxidation	m^3 mol^{-1} s^{-1}

r	Reaction rate	mol m^{-3} s^{-1}
$r_{C_2H_5OH\ dehydro}$	C_2H_5OH dehydrogenation rate of reaction	mol m^{-3} s^{-1}
$r_{CH_3CHO\ dec}$	C_2H_3CHO decomposition rate of reaction	mol m^{-3} s^{-1}
$r_{CH_3CHO\ ox}$	C_2H_3CHO oxidation rate of reaction	mol m^{-3} s^{-1}
$r_{C_2H_5OH\ ox}$	C_2H_5OH oxidation rate of reaction	mol m^{-3} s^{-1}
$k^{inh}_{C_2H_5OH\_1}$	C_2H_5OH dehydrogenation self inhibition coefficient	m^3 mol^{-1}
$k^{inh}_{C_2H_5OH\_2}$	C_2H_5OH oxidation self inhibition coefficient	m^3 mol^{-1}
$k^{inh}_{CH_3CHO\_1}$	CH_3CHO decomposition self inhibition coefficient	m^3 mol^{-1}
$k^{inh}_{CH_3CHO\_2}$	CH_3CHO oxidation self inhibition coefficient	m^3 mol^{-1}
$k^{inh}_{CO\_1}$	CH_3CHO decomposition – CO inhibition coefficient	m^3 mol^{-1}
$k^{inh}_{CO\_2}$	CH_3CHO oxidation – CO inhibition coefficient	m^3 mol^{-1}
$k^{inh}_{CO\_3}$	C_2H_5OH oxidation – CO inhibition coefficient	m^3 mol^{-1}
$k^{inh}_{NO\_1}$	CH_3CHO decomposition – NO inhibition coefficient	m^3 mol^{-1}
$k^{inh}_{NO\_2}$	CH_3CHO oxidation – NO inhibition coefficient	m^3 mol^{-1}
$k^{inh}_{NO\_3}$	C_2H_5OH oxidation – NO inhibition coefficient	m^3 mol^{-1}
R	Universal gas constant	J/molK
T	Surface temperature	°C
[X]	concentration of a reactant X	mol m^{-3}

Abbreviations and Acronyms

AFR	Air fuel ratio
cpsi	Cells Per Square Inch
E85	85% Ethanol and 15% Gasoline Fuel
FTIR	Fourier Transform Infrared Spectroscopy
HC	Hydrocarbon
JLR	Jaguar Land Rover
PdRh	Palladium and Rhodium Catalytic Converter Formulation
PtRh	Platinum and Rhodium Catalytic Converter Formulation
ppm	Parts Per Million
ppmC	Parts Per Million Carbon

SI	Spark Ignition
TWC	Three-way Catalyst
THC	Total Hydrocarbons

Chemical Symbols

CH_4	Methane
C_3H_6	Propylene
C_3H_8	Propane
CH_3CHO	Acetaldehyde
CH_3OH	Methanol
C_2H_5OH	Ethanol
CO	Carbon monoxide
CO_2	Carbon dioxide
H_2	Hydrogen
H_2O	Hydrogen
N_2	Nitrogen
NO	Nitric oxide
NO_x	Oxides of nitrogen
O_2	Oxygen
Pd	Palladium
Pt	Platinum
Rh	Rhodium

Acknowledgements

This work was supported by the Department of Education and Learning, and the authors would like to thank Jaguar Land Rover for financial support.

References

1. Yanowitz J, McCormick RL. Effect of E85 on Tailpipe Emissions from Light Duty Vehicles. J. Air Waste Manage. Assoc. 2009; 59: 172-182.

2. Zarante P, Costa T and Sodre J. Aldehyde emissions from an ethanol-fuelled spark ignition engine: Simulation and FTIR measurements. Blucher Chem. Eng. Proc. 2015; 1, 7738–7745.

3. West BH, Lopez AJ, Theiss TJ, et al. Fuel Economy and Emissions of the Ethanol Optimised Saab 9-5 Biopower. 2007, SAE paper no. 2007-01-3994.

4. Brusstar MJ, Gray CL Jr. High Efficiency with Future Alcohol Fuels in a Stoichiometric Medium Duty Spark Ignition Engine. 2007, SAE paper no. 2007-01-3993.

5. Kar K and Cheng WK. Speciated Engine-Out Organic Gas Emissions from a PFI-SI Engine Operating on Ethanol/Gasoline Mixtures. SAE Int. J. Fuels Lubr. 2010; 2(2): 91-101.

6. Kar K, Tharp R, Radovanovic M, et al. Organic gas emissions from a stoichiometric direct injection spark ignition engine operating on ethanol/gasoline blends. Int. J. Engine Res. 2010; 11: 499-513.

7. Lupescu J, Chanko T, Richert J, et al. Treatment of Vehicle Emissions from the Combustion of E85 and Gasoline with Catalyzed Hydrocarbon Traps. SAE Int. J. Fuels Lubr. 2009; 2(1): 485-496.

8. Manzetti S, Andersen O. A review of emission products from bioethanol and its blends with gasoline. Background for new guidelines for emission control. Fuel. 2015; 140: 293–301.

9. Suarez-Bertoa R, Zardini A, Keuken H, et al. Impact of ethanol containing gasoline blends on emissions from a flex-fuel vehicle tested over the Worldwide Harmonized Light duty Test Cycle (WLTC). Fuel. 2015; 143: 173-182.

10. Zarante P, Sodré J, Simulation of Aldehyde Emissions from an Ethanol Fueled Spark Ignition Engine and Comparison with FTIR Measurements. Journal of Physics: Conference Series 745 (2016) 032023

11. Maunula T and Kinnunen T. Effect of Oxygen Containing Biofuels on the Emissions with Exhaust Gas Catalysts. 2009, SAE paper no. 2009-01-2737.

12. Stepane J, Koci P, Marek M, et al. Effects of Biofuel Blends on Performance of Exhaust Gas Catalyst: Ethanol and Acetaldehyde Reactions. SAE Int. J. Fuels Lubr. 2010; 3(1): 523-536.

13. Guarido CEM, Souza M and Schmal M. A Study of Ethanol Reactions over Pt/Al2O3 and Pt/ZrO2 by Temperature-Programmed Surface Reactions. ENPROMER Second Mercosur Congress on Chemical Engineering, 2005.

14. Falthali, A and Esktrom M. Methane Production over Three-Way Catalysts in E85-Fuelled Vehicles. 2011, SAE Paper no. 2011-01-0643.

15. Kuo JCW, Morgan CR and Lassen HG. Mathematical Modeling of CO and HC Catalytic Converter Systems. 1971, SAE Paper no. 710289.

16. Voltz SE, Morgan CR, Liederman D, et al. Kinetic Study of Carbon Monoxide and Propylene Oxidation on Platinum Catalysts. Ind. Eng. Chem. Prod. Res. Dev., 1973, 12(4), 294-301.

17. Montreuil C, Williams S and Adamczyk A. Modelling Current Generation Catalytic Converters: Laboratory Experiments and Kinetic Parameter Ptimization - Steady State Kinetics. 1992, SAE Paper no. 920096.

18. McAtee C, McCullough G and Douglas R. Performance and characteristics of platinum, palladium/rhodium and palladium automotive catalysts when subjected to ethanol, acetaldehyde and a synthetic E85 exhaust gas mixture. Proc IMechE Part D: J Automobile Eng. 2012; 226: 1536-1546.

19. McAtee C, McCullough G, Douglas R et al. The Effect of De-Greening and Pre-Treatment on Automotive Catalyst Performance. 2011, SAE paper no. 2011-24-0188.

20. www.exothermia.com [viewed on 13 Nov 2018]